Numerical Development of a Coupled One-Dimensional/Three-Dimensional Computational Fluid Dynamics Method for Thermal Analysis With Flow Maldistribution

Haimi Jordaan, P. Stephan Heyns, Siamak Hoseinzadeh

Centre for Asset Integrity Management, Department of Mechanical and Aeronautical Engineering, University of Pretoria, Pretoria 002, South Africa

Email: u14227038@tuks.co.za
Email: stephan.heyns@up.ac.za
Email: Hosseinzadeh.siamak@up.ac.za

Abstract

This work describes the development of a methodology that couples one-dimensional (1D) network elements with three-dimensional spatial computational fluid dynamic (CFD) elements to analyze shell-and-tube heat exchangers with dense tube bundles. The 1D elements represent the tube flow while the spatial elements represent the external auxiliary flow. This reduces the computational expense significantly as compared to full computational fluid dynamics analysis of the same system, while a detailed transient temperature distribution can still be obtained. The methodology uses a unique combination of relaxation algorithms, a polynomial regression mapping procedure, and discretisation methods to create a coherent numerical methodology. Simulations are performed on a TEMA-FU-type shell-and-tube heat exchanger. The methodology was validated against full CFD and indicates errors between the calculated logarithmic mean temperature differences (LMTD) of less than 2% over a range of turbulent flow conditions. Various combinations of media for primary and auxiliary fluids are considered, to test the applicability and robustness of the methodology. Finally, a transient simulation of timed step inputs for the flowrate and temperature of both primary and auxiliary fluids also corresponds with a full CFD analysis. It is concluded that the proposed 1D-CFD method is effective for simplifying the analysis of flow-through tube bundles.

Keywords: heat and mass transfer, heat exchangers, CFD

1 Introduction

There is a need in the power industry for improved analysis of specific failures in tubesheet-type feedwater heaters. A feedwater heater is a common component in most power plants and is used to improve the cycle efficiency by preheating the feedwater to the boiler. It has a dense tube bundle, and comprehensive computational fluid dynamics (CFD) analysis is impractical due to its large size. Feedwater heater tubesheets are susceptible to thermal fatigue failures due to power plant cycling that induces mass flow, pressure, and temperature transients. The rate of power plant cycling, and consequential fatigue failure, is increasing substantially as renewable energies are further developed and implemented.

Improved understanding of these fatigue failures requires numerical thermal analysis [1]. Detailed transient temperature distribution of the tubesheet is essential. In the past, researchers have used finite element methods (FEM) that require specified boundary

conditions at the structural surface. These specified boundaries can be obtained by using on-site measurements [2], but this is not always practical and crude assumptions are commonly made. Examples of such assumptions include uniformly assigned temperatures on the shell-and-channel side [3,4] or assumed convection coefficients [5,6]. CFD together with fluid–structure interaction (FSI) offers engineers the capability to obtain detailed transient temperature and stress distributions, but typically with a large computational cost if the models are substantially large and complex.

This paper presents a methodology to reduce the CFD computational expense by modeling the internal tube walls and flow with one-dimensional (1D) network elements while utilizing spatial CFD elements for the complex shell-side flow. Three different types of 1D-CFD cosimulation methods exist as described by Ref. [7] and can be listed as follows:

1. fully separated model;
2. hydraulically unified model; and
3. hydraulically disconnected model.

The fully separated model has no direct coupling between the spatial and network elements. CFD products are often employed to obtain a response surface or train an artificial neural network [8] to provide inputs for another component. The hydraulically unified model couples only the inlet and outlet boundary conditions of a spatial CFD model with the 1D network. It is the most popular of the methods as it allows for a wide range of input parameters to be simulated when constructing a response surface is impractical. Finally, a hydraulically disconnected model consists of 1D network elements that penetrate the spatial domain. The proposed methodology is classified as a hydraulically disconnected method.

There have been many studies that entail thermal analyses of shell-and-tube heat exchangers (STHX) by solely using 1D network models. For instance, the work of Ref. [9] focused on object-oriented modeling of an STHX for concentrated solar power. Reference [10] described the application of a 1D thermofluid network approach to model a superheater heat exchanger with a complex flow arrangement. Several models of varying complexity that are based on object-oriented modeling which obtained good agreements to experimental results have also been summarized [11]. These models are adequate for well-defined heat exchanger geometries and flow characteristics but fall short when there are flow inconsistencies or when detailed results are required. By utilizing CFD, these inconsistencies can be addressed. Examples include the investigation of baffle arrangements and spiral tubes for which empirical correlations do not exist [12,13]. CFD has proven to be effective and accurate but are only practical for simple STHX models or by incorporating high-performance computing for large problems, which does not always guarantee that the problem is tractable. Using a thermal porous media model was recently shown to be promising to reduce computational effort but is also restricted to basic auxiliary flows [14].

Surprisingly, not many studies exist in the literature that utilize hydraulically disconnected cosimulation as is proposed here. However, some studies have been found in which a 1D-CFD approach is used to model a coal-fired boiler at a power station [15]. They implemented the 1D network to represent the internal flow of the tubes and CFD for the external flow. The same authors supervised a study on the feasibility of using a 1D-CFD method to model an air-cooled heat exchanger, which reported good accuracy compared to a full CFD model [16]. Although they used similar principles, the coupling and mapping procedure in the proposed

methodology differs substantially and has been significantly developed in this work to account for maldistribution and/or transient loadings.

This study uses a least-squares polynomial mapping procedure between solvers for continuous transfer variables. It also incorporates a method to analyze flow maldistribution by utilizing 1D flow elements. Furthermore, two discretisation methods of lumping 1D and 3D elements are described that are unique to this methodology. Although many of these methods have been developed in their regard by others, the combination and utilization of these on a similar scale has not been found elsewhere. This study aims to describe a multiscale 1D-CFD method that can be used to simplify the thermal characteristics of a tube bundle. The model is tested by varying the inlet flow conditions, media, and transient step inputs. The temperature along the tubesheet and the outlet temperature distribution are deemed the key performance indicators of the method. These are evaluated by comparing it with a full CFD version of the model.

Experimental validation is not considered relevant for this work. We depart from the premise that a full CFD analysis will generally better capture the underlying physics of the problem under consideration than a simplified 1D-CFD counterpart. The principal aim of this work is therefore to compare the performance of the proposed simplified 1D-CFD computational approach to that of a full CFD, which may be viewed as the best that one can reasonably achieve through computational means. In this work, we therefore do not address the question of the extent to which the full CFD really captures the underlying physics of the problem.

In this paper, we also opt to consider a geometry that is sufficiently simple so that multiple cases can be tested while containing complexities such as tube flow maldistribution and geometric features. This simple theoretical geometry is presented in this paper to demonstrate and validate the methodology that was later applied practically to a feedwater heater consisting of 560 tubes.

In this work, we use flownex and ansys fluent for the 1D network solver and CFD solver, respectively. Flownex is a component-based thermal-hydraulic network solver that has proven its worth in the nuclear industry [17]. It solves the conservation of mass, momentum, and energy, which are simplified into 1D representations. These governing equations for flow in a pipe are given by Eqs. (1)–(3) representing continuity, momentum, and energy respectively

$$\frac{\partial \rho}{\partial t} + \frac{\partial}{\partial x}(\rho V) = 0 \tag{1}$$

$$\frac{\partial (\rho V)}{\partial t} + \frac{\partial (\rho V^2)}{\partial x} = -\frac{\partial p}{\partial x} - \rho g \frac{\partial z}{\partial x} - \frac{f \rho |V| V}{2D} \tag{2}$$

$$\frac{\partial (\rho (gz) - p)}{dt} + \frac{\partial (\rho V (h_0 + gz))}{dx} = \dot{Q}_H - W \tag{3}$$

Flownex has a built-in link to ansys fluent by modifying parameters and scheme variables within Fluent's text user interface (TUI). ansys fluent is a very well-known commercial CFD software that is capable of simulating conjugate heat exchangers effectively. The 3D CFD governing equations built into Fluent are well documented [18] and are not repeated here. As the 3D governing equations pertain to the external shell-side flow, the near-wall treatment between the reduced 1D–3D model and the full 3D model is consistent. This means that the

methodology can be applied to various combinations of CFD models provided that the tube flow is appropriately approximated.

2 Methodology

The proposed methodology is simple and inspired by conjugate heat transfer methods. The main aspects of the methodology are the zone discretisation, mapping, and coupling process and are subsequently described.

2.1 Discretisation

The heat transfer characteristics in various zones of a heat exchanger can differ substantially. Examples include the cross-flow and parallel flow zones. For discretisation, we employ the following terminologies in the present work. In descending hierarchal order, we introduce

- A *mass flow group* as a set of tubes that have comparable mass flows that are lumped.
- A *segment*, which refers to tubes that are consistent in geometry and in flow characteristics. For instance, a straight tube, U-bend, sensible heat transfer, and condensing flow would each be represented by a different segment.
- *Sections* are lumped zones used to define the mapping polynomial curve of the transfer variables along a segment.

Two methods were identified to discretise the flow domain to account for variations in the heat transfer rates.

The first discretisation method is referred to as *flow group discretisation* which divides assigned flow groups into sections that might be of particular interest. This discretisation method is useful when flow maldistribution must be considered. Every flow group requires at least one different segment. A simple example of this method is depicted in Fig. 1, which shows two flow groups, each with one segment and five sections located at zones of interest. These zones can be of any size provided that the flow groups remain separated. This means that sections cannot cross from one flow group to another as is possible in the next discretisation method. The cases simulated in this paper use *flow group discretisation* as significant maldistribution exists within tubes.

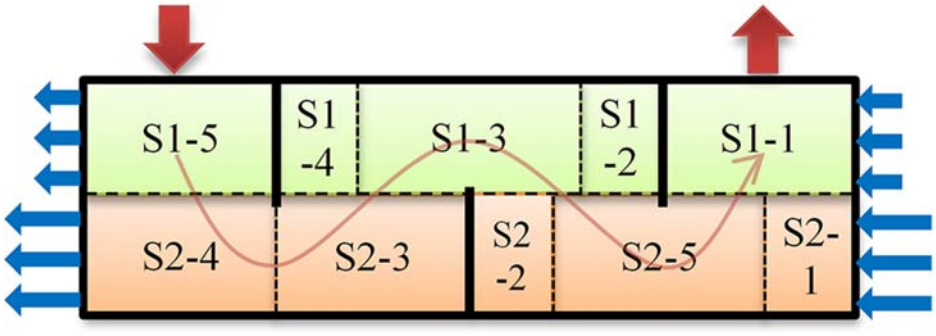

Fig. 1. Flow group discretisation example

The second method is referred to as the *Characteristic Discretisation* method, as the location of defined zones depends on the characteristics of the flow within those zones. For instance, a domain can be discretised in cross-flow and window-type zones in a baffled STHX [9]. This discretisation method is useful when precise control over the primary fluid temperatures is required when complex geometries and additional heat transfer phenomena on the shell side need to be considered. Unlike the *flow group discretisation*, this method must assume a uniform mass flow within tubes as the determination of maldistribution is not possible. In Fig. 2, an example of this method is illustrated, which shows segments assigned to expected cross-flow (X) and counterflow (C) zones, respectively. Its equivalent 1D network model is shown in Fig. 2.

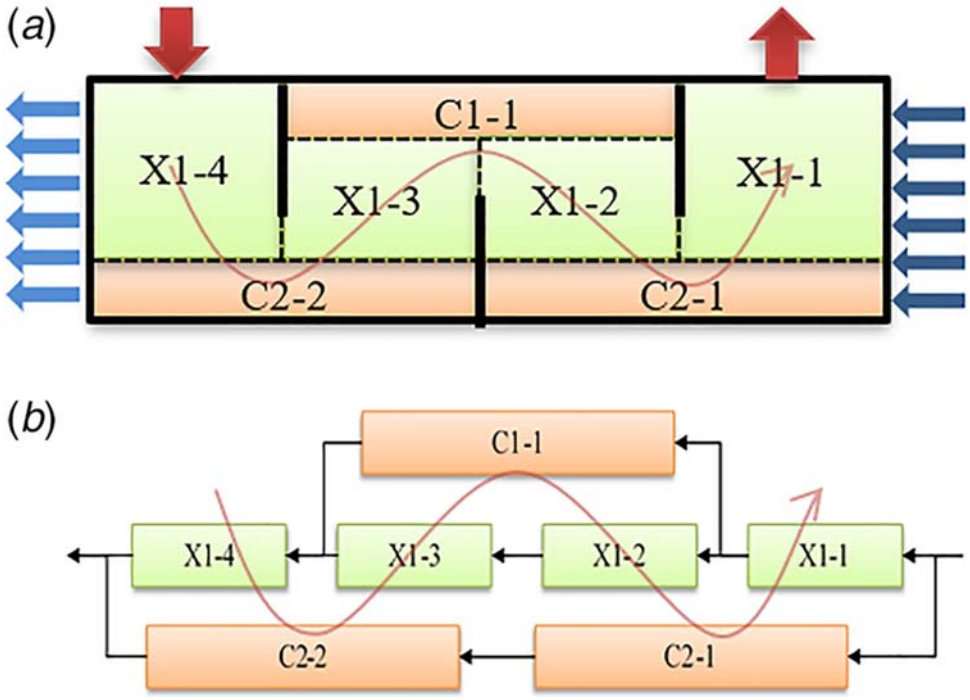

Fig. 2. (*a*) Heat transfer discretization counter- and cross-flow zone layout and (*b*) 1D tube-side network representation

2.2 Mapping

The variables are mapped to the boundaries by means of fitted regression polynomials. The coefficients of these polynomials are obtained from averaged values from each of the defined sections. This approach is only valid if the internal temperatures along the tubes are monotonically increasing or decreasing. A polynomial is assigned to every segment and can be of any order depending on the situation. The benefit of utilizing approximating polynomials to transfer variables compared to uniform/discrete values is that it reduces discontinuities between segments, which can lead to solution instabilities. It is obviously also more accurate as well.

An example of the mapping procedure is graphically depicted in Fig. 3, which illustrates a single segment with multiple sections and arbitrarily obtained polynomial functions. The lumped sections do not require a uniform length, nor do nodes need to be conformal between

corresponding solvers. It is evident that the mapping is applied on a much larger scale using lumped sections, than by mapping on a node-to-node basis. This means that the methodology is not sensitive to the specific treatment of the near wall dictated by the model choice and results will be consistent between a 1D–3D coupled model and full CFD model, provided that the tube-side flow is appropriately approximated by the 1D elements. It should be noted that the tube wall can be represented with either 1D or 3D elements and be numerically solved with either of the solvers. A trade-off exists between higher detail and a lower computational time and must be based on the requirements of the problem.

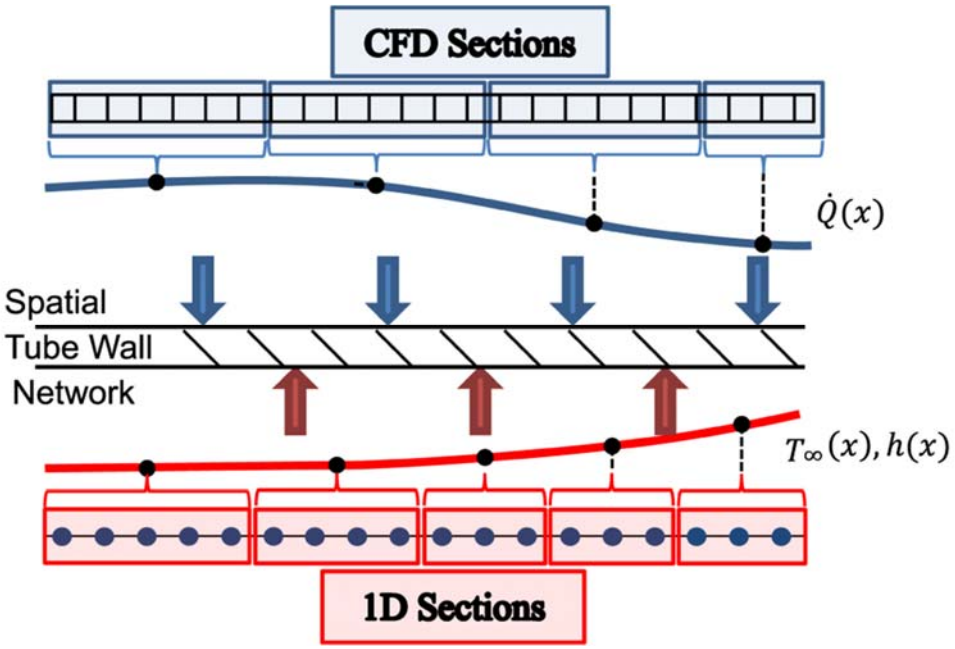

Fig. 3. Mapping procedure example schematic of 1D and CFD zones

2.3 Coupling Process

Two methods of thermal coupling exist [15]. The first is an implicit method in which a global matrix of coefficients is assembled and solved numerically. The second is an explicit method where the data are exchanged at regular intervals, and the variables within the solvers are kept separate. This study opted for the latter.

The solvers were thermally coupled by transferring calculated variables between solvers according to a procedure that is depicted in Fig. 4. The 1D network transfer variables are defined as the internal convection coefficient h and the bulk fluid temperature T_∞. These vary along the position of the tube, x. The internal convection coefficient $h(x)$ is calculated in this investigation (but is not limited to) using the well-known Gnielinski's correlation expressed in terms of the local Nusselt number as

$$\mathrm{Nu}(x) = \frac{(f/8)(\mathrm{Re} - 1000)\ \mathrm{Pr}}{1 + 12.7(f/8)^{0.5}(\mathrm{Pr}^{2/3} - 1)} \begin{pmatrix} 0.5 \leq \mathrm{Pr} \leq 2000 \\ 3 \times 10^3 < \mathrm{Re} < 5 \times 10^6 \end{pmatrix} \quad (4)$$

where Re and Pr are the dimensionless Reynolds and Prandtl numbers, respectively.

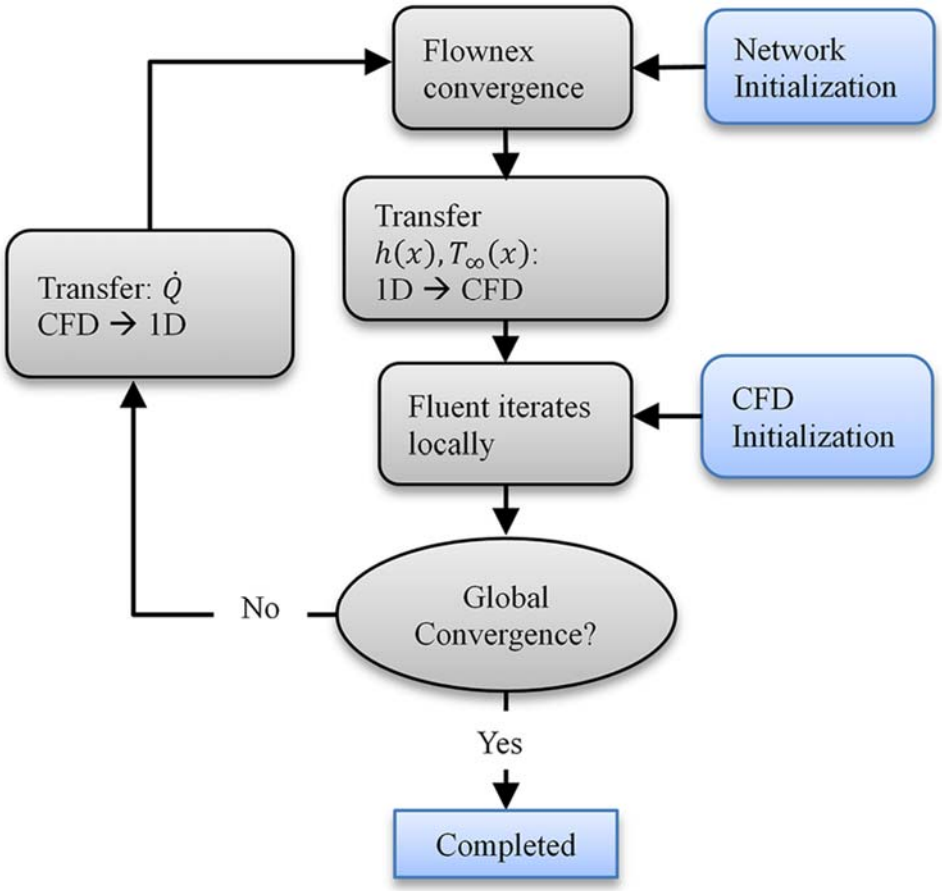

Fig. 4. Thermal coupling process

Flownex is always allowed to iterate to convergence, as doing so is computationally insignificant, and $h(x)$ and $T_\infty(x)$ are then transferred to Fluent. Fluent iterates through a specified number of iterations, which are referred to as local iterations. It was found that the number of local iterations affects the rate of convergence and therefore the computational time. Here, the authors opted to use 10 local iterations before triggering a global iteration. This was determined through a trial-and-error approach. The selected number of iterations must be large enough to ensure that thermal variables stabilize, whilst small enough to avoid excessive iteration that reduces the efficacy of the methodology. For example, transferring data after each local iteration will often result in solution instabilities and too many iterations lead to very slow global convergence between solvers. A global iteration refers to the transfer of data between solvers.

The system typically converges after several global iterations. Global convergence is attained when changes in transfer variables are negligibly small, and if Flownex and Fluent have also locally converged. To improve stability and convergence, relaxation coefficients were implemented. The thermal relaxation coefficient ξ_t was set to 0.8, which corresponds to the coefficient used in Ref. [19] in their conjugate heat transfer algorithm. The transient simulation uses nearly the same procedure as the steady-state case. The only addition is the

implementation of the Gauss–Seidel scheme for global iterations. This scheme was selected for its simplicity.

2.4 Flow Maldistribution

In addition to thermally coupling 1D and spatial CFD elements, similar principles were used to develop a method to analyze flow maldistribution in tube bundles, by coupling 1D–3D elements. Flow maldistribution is common in heat exchangers and can adversely affect heat transfer. Both thermal and flow coupling can be implemented simultaneously, which was done for the cases in this work. Network models have previously been employed to analyze complex flow arrangements [14] and are certainly capable to do so for a tube bundle.

The proposed method again utilizes the coupling of 1D network elements to spatial elements in order to reduce computational expense, but the interface of 1D elements and 3D CFD elements are completely different from that of the thermal coupling. The flow–coupling interface is illustrated in Fig. 5. As depicted, the heat exchanger channel-side is modeled with spatial CFD elements and only a small length of the tube inlets to ensure the flow develops hydraulically and thermally. Biased flow can exist based on the conditions of the problem. For example, the impinging flow on the bottom plate of the channel inlet creates positive pressure for the flow into the lower row of tubes. This increases the flowrate but also the primary pressure loss in these tubes. Furthermore, secondary losses from geometrical parameters, like the bend radius, affects the pressure loss. The resulting overall pressure coefficient K_i is therefore different for many tubes and can cause significant maldistribution of flow.

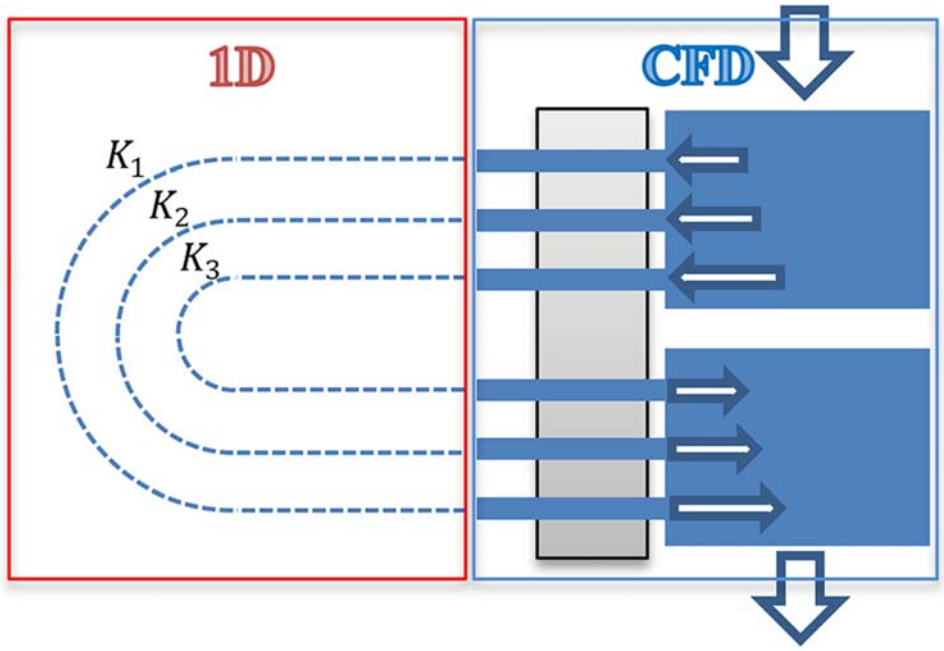

Fig. 5. Tube-side flow maldistribution coupling schematic

In this study, we used Flownex to calculate the pressure drop, using the Darcy friction factor for turbulent flow, with:

$$f = 8\left(\frac{V_*}{V}\right)^2 \quad (5)$$

$$V_* = \sqrt{\frac{\tau_0^{guess}}{\rho}} \quad (6)$$

where τ_0 is the local shear stress that can be approximated numerically with the Herschel–Bulkley fluid model. Secondary pressure losses are also accounted for with the use of Flownex's empirical correlation components. The tubes are lumped into several groups, and the number of groups depends upon the desired level of resolution.

A global iteration occurs when each flow group transfers the obtained pressure loss to Fluent as backpressure, which then computes the new mass flowrate of each flow group. This is an iterative process, and the relaxation coefficient ξ_p was set to 0.15, which is very stiff in comparison with ξ_t as a strong implicit dependency between flow variables exists. The stiff relaxation coefficient stabilizes the solution but reduces the convergence rate.

3 Setup

To test the strategy, an STHX model was designed to resemble a feedwater heater. A Tubular Exchanger Manufacturers Association (TEMA) of FU type that consists of U-tubes and a double longitudinal pass was deemed suitable. Baffles were also placed along the tubes on the shell side. Usually, a feedwater heater consists of hundreds of tubes. This model was simplified to only 18 tubes to reduce the simulation time and accelerate the development of the methodology. As previously mentioned, the methodology was later applied to a feedwater heater consisting of 520 tubes. The full geometry can be seen in Fig. 6. The primary and auxiliary fluid flows are in a counterflow orientation. Table 1 provides geometric parameters.

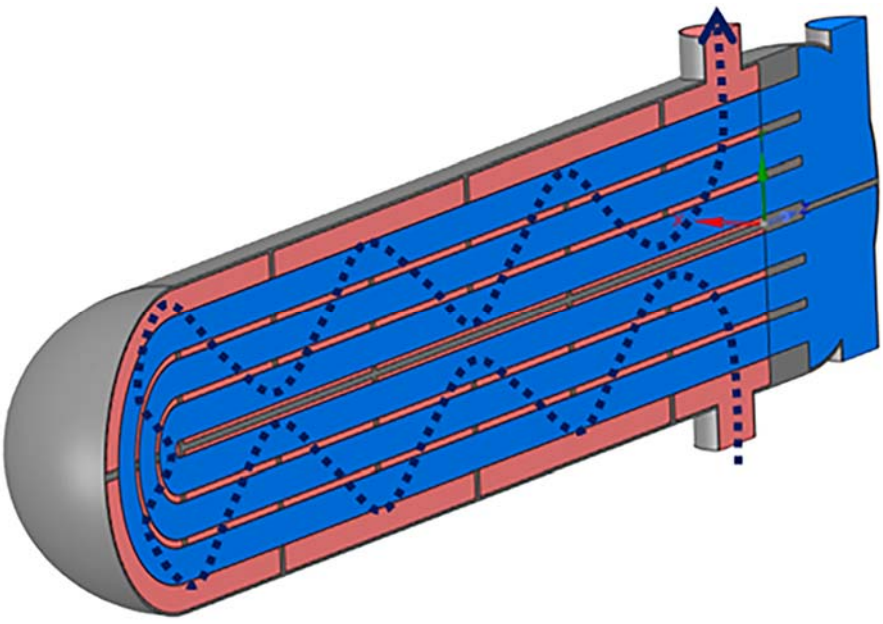

Fig. 6. TEMA-FU CAD geometry

Table 1

Assigned geometric parameters of TEMA-FU type

Property	Symbol	Size (mm)
Outer diameter	D	10*d*
Shell thickness	t_s	0.1*d*
Tubesheet thickness	t_t	2.5*d*
Tube inner diameter	*d*	–
Shell length	*L*	38*d*
Material	–	Stainless steel

3.1 Computational Fluid Dynamics

The difference between the coupled 1D-CFD and the full CFD approach is the implementation of transfer variables, and there is no mesh for the internal flow in the 1D-CFD method. The transfer variables are defined by means of the Fluent parameters and/or scheme variables. The pressure-based solver was utilized wherein the constraining of mass conservation of the velocity field is achieved by solving the pressure equation [18]. The Coupled Pseudo-Transient SIMPLE algorithm was selected as the solution method. The internal tube flow was simulated for various turbulent cases. The viscous sublayer could not be resolved due to the available computing power. It was, therefore, decided to use wall functions. The *k*-epsilon realizable model was selected based upon its features, that is, its superiority to capture the mean flow of complex structures compared to the standard formulation. Scalable wall functions were used with obtained *y*+ values ranging between 43 and 70 on all wall boundaries.

3.1.1 Boundary Conditions

The inlet to the STHX has specified a fully turbulent power-law velocity profile and was implemented using a user-defined function (UDF) in Fluent. The standard one-seventh power-law velocity profile

$$\frac{\bar{v}}{V_{\max}} = \left(1 - \frac{r}{R}\right)^{1/n} \tag{7}$$

was used with an exponent $n = 7$, with the assumption that the flow was fully developed at the inlet. The inlet turbulence conditions at the inlet could be described in terms of the turbulence intensity and the hydraulic diameter. The inlet turbulence intensity was calculated with the expression [18]

$$I = 0.16\,\mathrm{Re}_{d_h}^{-1/8} \tag{8}$$

where Re_{d_h} is the Reynolds number based on the pipe hydraulic diameter. The symmetry boundary condition was applied to the symmetry plane of the STHX, which assumes a zero flux of all quantities across the boundary. A no-slip condition was prescribed on the walls, with all the external shell walls being thermally insulated.

3.1.2 Mesh

The mesh of the problem was generated using Fluent ICEM meshing. The details of the mesh can be seen in Fig. 7. The mesh consists predominantly of hexahedral elements. The mesh shown is that of the full CFD case. The mesh consists of approximately 7.5 million finite volume cells. In the 1D-CFD model, the internal flow and tube walls do not mesh, and therefore, the size of the mesh is reduced by approximately 40% for this specific model.

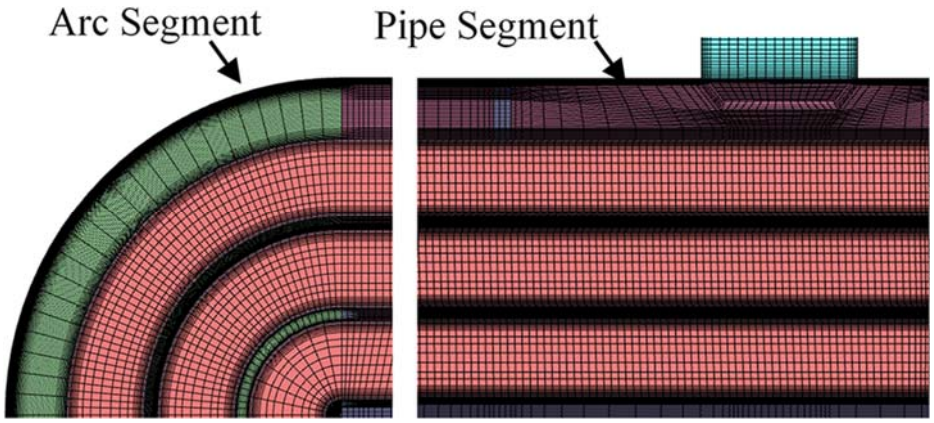

Fig. 7. Mesh of TEMA-FU

A mesh independence study was performed as described by Roache [20]. The evaluating variables were selected to be the outlet temperatures of the primary and auxiliary fluids. An acceptable mesh consisting of 3.2 million cells was selected based on the grid convergence index (GCI).

3.2 Network Solver

The network solver layout for a single segment can be seen in Fig. 8. Multiple segments in the STHX may exist, and these network solver modules are concatenated. Many components within the network layout can be seen in Fig. 8. The *Excel* component summarizes and stores the transfer data. These data are transferred to the Fluent component that utilizes its TUI to adjust the defined parameters and scheme variables before triggering a global iteration. The *Script* component implements the relaxation coefficients, convergence criteria, and non-standard adjustments. It would be laborious and unnecessary to explain each data transfer link (DTL) but the primary transfers, as depicted in Fig. 4, are $\dot{Q}$—DTL#4 and $h(x)$ and $T_\infty(x)$—DTL#2.

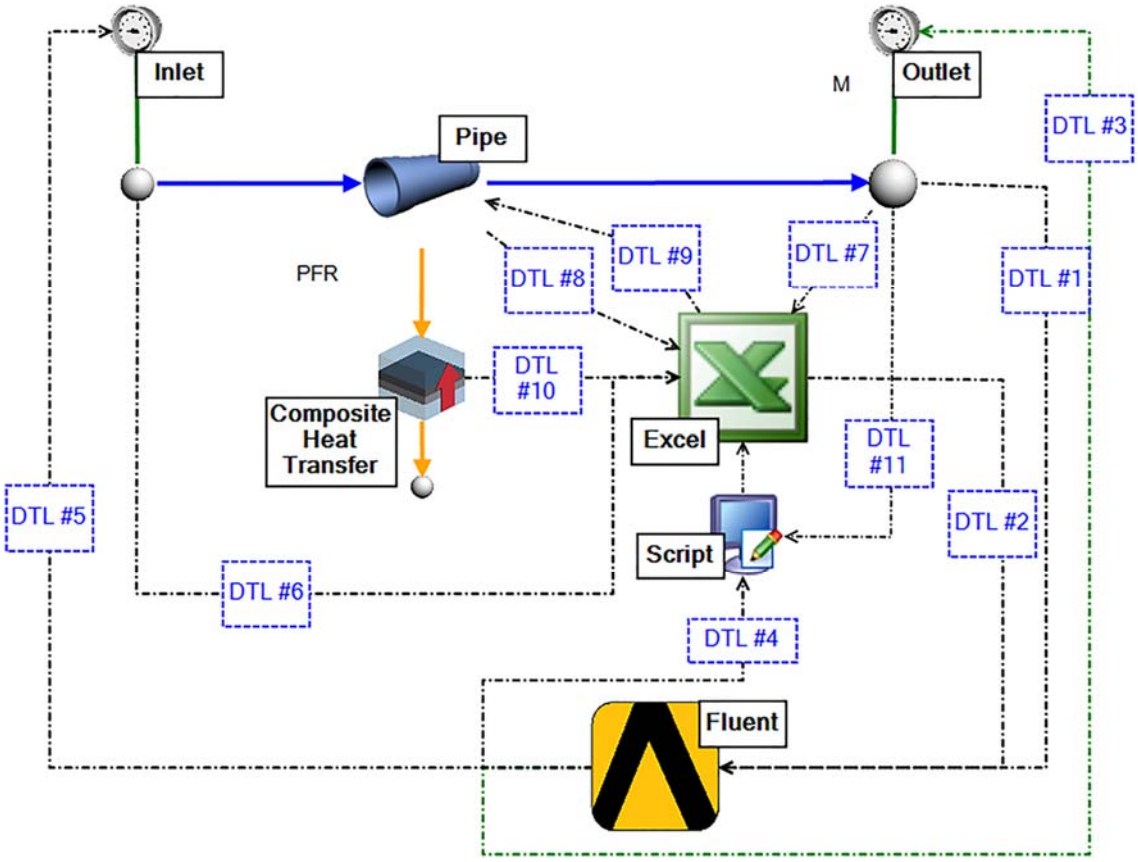

Fig. 8. Flownex network of a single segment

In the proposed model, each flow group consisted of three such segments in series, which represent the straight tubes and the bend. The two straight segments consisted of three sections each, from which the heat transfer rate $\dot{Q}$ along the STHX from Fluent was obtained. The bend was assigned only one section due to its small area.

4 Results and Discussion

The methodology was tested by varying the Reynolds number, the fluid media, and by performing transient simulations for stepped inputs. These tests are presented sequentially, and the 1D-CFD coupled method is compared throughout with the full CFD.

4.1 Reynolds Number

The outlet temperature of the primary and auxiliary fluids was evaluated, as well as the tubesheet temperature distribution along the symmetry plane. Contours of the velocity distribution are presented to validate the flowrate group assignment. The first set of simulations pertains to the variation of the primary fluid. The primary and auxiliary fluid is specified as liquid with temperature-dependent thermal properties. The error between the 1D-CFD coupled approach and full CFD was based upon the logarithmic mean temperature difference (LMTD) commonly used for heat exchanger calculations which is given by:

$$\Delta T_{lmtd} = \frac{\Delta T_1 - \Delta T_2}{\ln\left(\frac{\Delta T_1}{\Delta T_2}\right)} \quad (9)$$

where $\Delta T_1 = T_{h_i} - T_{c_i}$ and $\Delta T_2 = T_{h_e} - T_{c_e}$ and the subscripts *h* and *c* denote the hot and cold fluids, respectively. Three cases were simulated with varying Reynolds numbers. The inlet temperatures of the primary and auxiliary fluid for each case were 5 °C and 170 °C, respectively. This indicates that the auxiliary flow is under high pressure to remain in a liquid state. The results are presented in Table 2 and summarize for each case the primary and auxiliary fluids denoted with subscripts *p* and *a*, respectively.

Table 2

Variation of primary fluid Reynolds number results for STHX

Tube Re	CFD (°C)	1D-CFD (°C)	Error
	LMTD	LMTD	
7000	107.13	109.13	1.86%
12000	103.11	104.59	1.43%
17000	99.66	100.94	1.29%

The results of the three cases agree very well with a slight improvement in accuracy as the Reynolds number increases. All the cases indicate that the 1D-CFD approach estimates slightly less heat transferred, compared to the full CFD. We believe that the reason for this is that the enhanced heat transfer rate from the additionally induced turbulence within the bend and downstream thereof was not accounted for. This reasoning is supported by the consistent decrease in the error as the Reynolds number increases and the secondary flows resulting from the bends become less significant.

Figure 9 graphically presents the distribution on the tubesheet where the negative *x*-values correspond to the side of the tubesheet where the primary fluid exits. Figure 9(a) illustrates the location of the pitches and also a summary of the problem for a referral. Figures 9(b)–9(d) indicate each of the pitch comparisons between the methods. A good agreement between the results can be observed, especially in the positive *y*-value region. More notable discrepancies exist at the side of the tubesheet where the primary fluid outlets, with temperatures of both the steam and channel side slightly lower for the 1D-CFD method. The reason is that the downstream primary fluid has consecutive errors along the tubes and it greatly influences the temperature of the tubesheet. The largest temperature difference is approximately 5 °C.

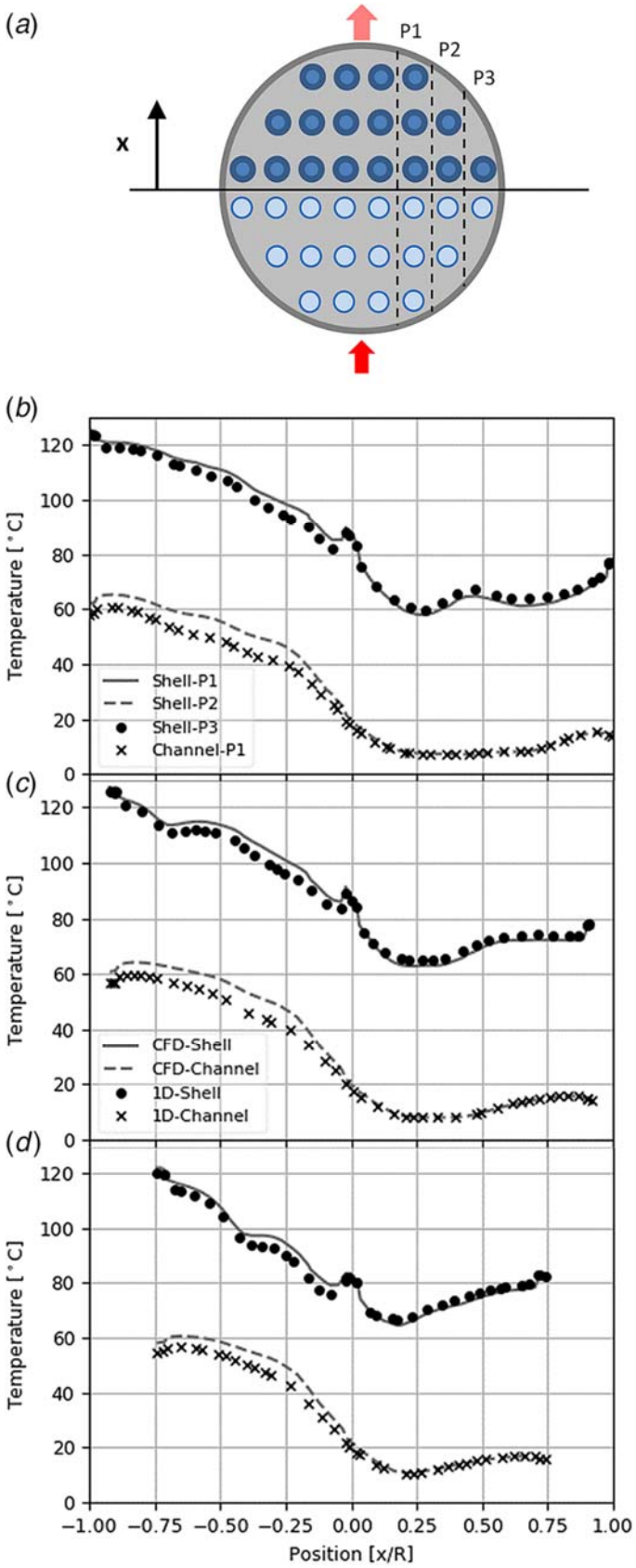

Fig. 9. Tubesheet temperature distribution results: (*a*) illustration of pitch location, (*b*) Pitch 1 (P1), (*c*) Pitch 2 (P2), and (*d*) Pitch 3 (P3)

The reduction in computational time for each case was consistently approximately 42%. This is predominantly due to the reduced mesh size of the 1D-CFD method which was 61% of the full CFD mesh. The method also used fewer iterations for the solution to converge which was due to the simplification of the internal flow. However, transferring variables from Fluent to Flownex during a global iteration incurs computational expense, which can be significant if triggered excessively.

4.2 Media Variation

In the previous cases, liquid water was selected as both the primary and auxiliary fluids. The results in this section investigate the effects of media selection between air and water. This assesses the range of applicability of the proposed methodology by evaluating the response when different temperature gradients along the heat exchanger are present. The input parameters of the three simulated cases, in a primary-auxiliary fluid format, are presented in Table 3. Each of these cases is designed to obtain unique temperature distribution as evident in Fig. 10.

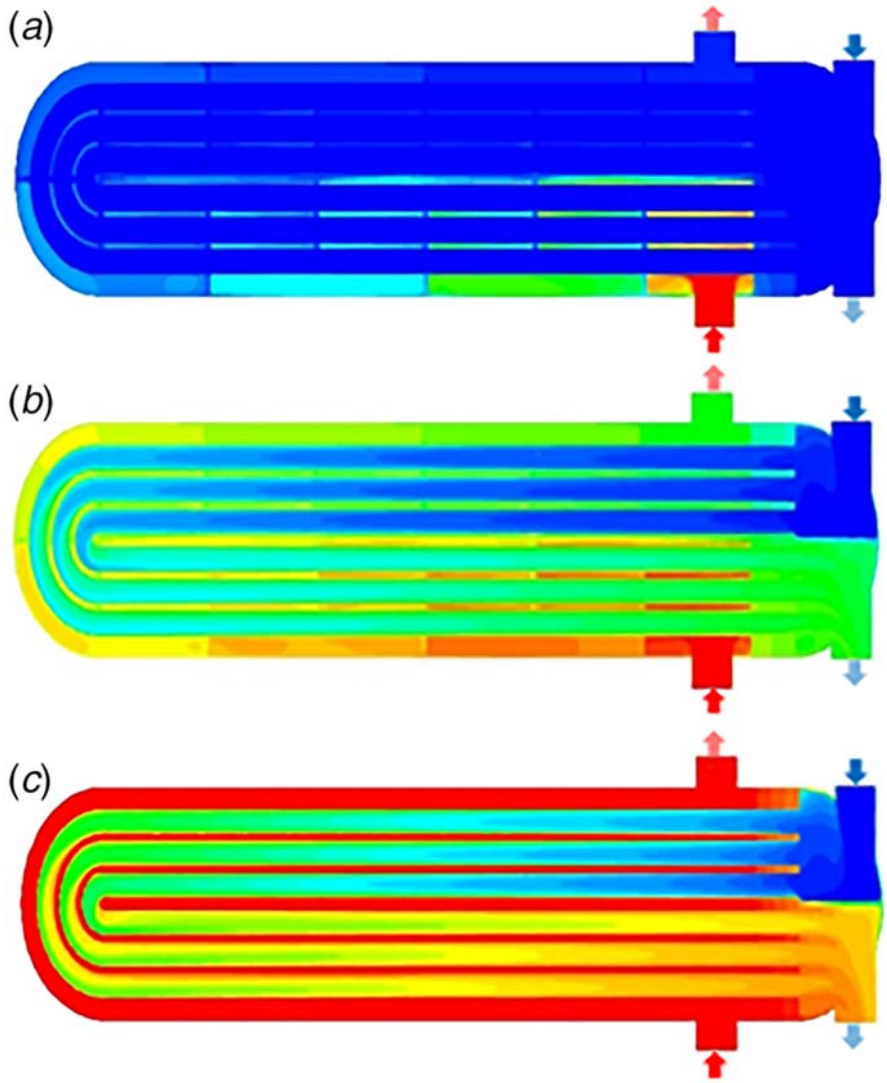

Fig. 10. Media variation symmetry temperature; (*a*) water–air, (*b*) air–air, and (*c*) air–wate

Table 3

TEMA-FU-type media variation case summary

Case	Primary fluid inlet		Auxiliary fluid inlet	
	T (°C)	Flowrate (kg/s)	*T* (°C)	Flowrate (kg/s)
Water–air	5	3	800	0.2
Air–air	5	0.1	800	0.1
Air–water	5	0.1	150	2

The cases were set up and simulated as described, from which a summary of the general heat exchanger results is presented in Table 4. The results indicate reasonable accuracy with the LMTD errors between the coupled 1D-CFD and full CFD approach reaching a maximum of 3%. Again, the LMTD of the coupled approach resulted in an underestimation of heat transfer.

Table 4

Media variation macroscopic results

Case	CFD (°C)	1D-CFD (°C)	Error
	LMTD	LMTD	
Water–air	258.42	261.24	1.09%
Air–air	404.28	416.43	3.00%
Air–water	74.36	74.72	0.48%

The contour plots of the CFD symmetry plane temperature for the three cases are presented in Fig. 10. It is evident that all the results indicated very different temperature distributions on the tubesheet. The temperature of the water remains relatively constant with changes of approximately 13 °C and 1 °C, while the air temperature changes drastically due to its lower thermal capacity. It was shown that the significant temperature gradients could be captured by the 1D approach by utilizing the polynomial mapping procedure as described previously in Sec. 2.2.

Similar to before, a more quantitative measure of results is presented by plotting the tubesheet temperature at position P1 for all three media variations and is provided in Fig. 11. It can be seen that the 1D-CFD temperature distributions align very well with the full CFD distributions for both the shell and channel side. The temperatures along the positive *x*-coordinates match exceptionally well due to the negligible change in temperature of the feedwater from its inlet. Downstream, the feedwater undergoes temperature variations and sequential errors are induced. The effects of the media on the temperature distribution are apparent by comparing the three different cases. In a realistic feedwater heater, the water–air case is most likely the best representation for the desuperheating zone, as hot air and superheated steam are comparable with regard to the thermal properties. The negative *x*-positions in Fig. 11(a) would be the critical region for thermal fatigue which corresponds to the steam inlet of a feedwater heater.

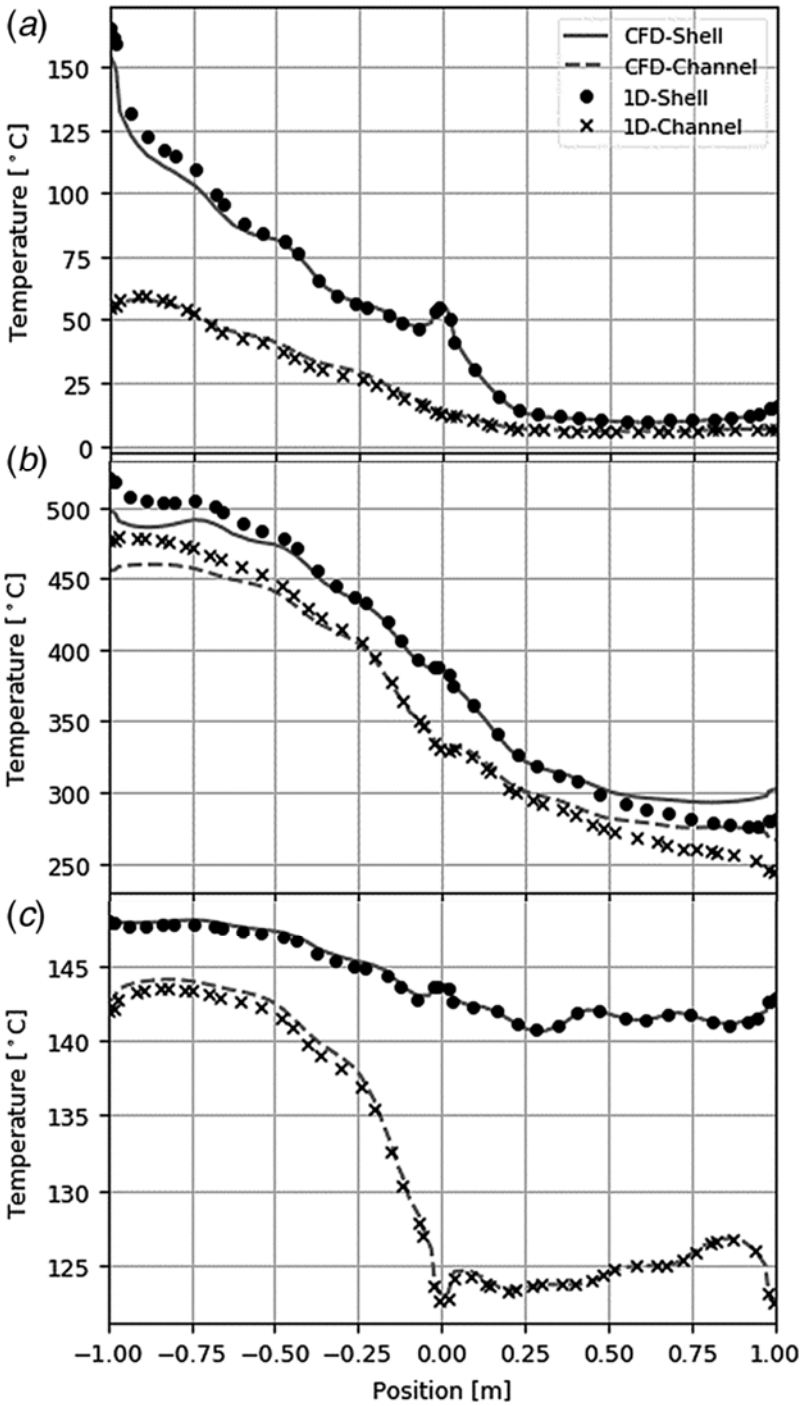

Fig. 11. Media variation tubesheet temperature distribution along P1: (*a*) water–air, (*b*) air–air, and (*c*) air–water

4.3 Transients.

Two different transient simulations of increasing complexity were performed. The first consisted of a temperature step in the inlet primary fluid. The second had temperatures and flowrates steps of both the primary and auxiliary inlets that are triggered at different times. The primary fluid propagates relatively slowly through the tubes in this model and in all cases required more than 50 s for a particle to travel through the heat exchanger. All the transient simulations were initialized from the steady-state case.

For the first case, a step input of 30 °C was chosen to easily observe the effects of the step. The step occurred at $t = 0$. The normalized outlet temperatures as given in Eq. (7) are presented in Fig. 12, for the 1D-CFD and full CFD methods.

$$\theta = \frac{T - T_{\min}}{T_{\max} - T_{\min}} \tag{10}$$

During the development of the proposed method, the results obtained from the transient simulations did not correspond well with the full CFD model. The spatial discretization of the 1D model had not been confirmed and was found to be the apparent reason for the errors. The number of 1D nodes, n, was increased from 5 to 44, and the results improved considerably as depicted in Fig. 12. The increase in computational expense was negligible.

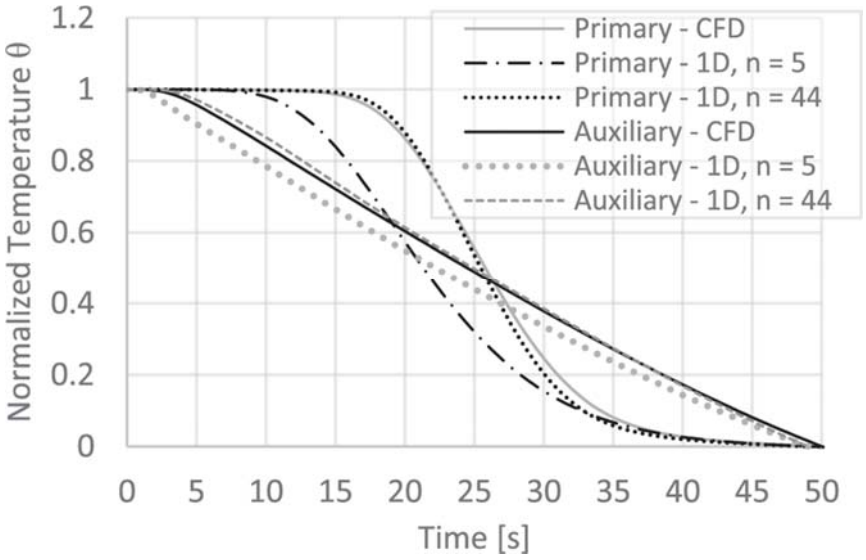

Fig. 12. Transient outlet temperature for a single applied step

For the second case, the temperature and mass flow inputs were stepped for both the primary and auxiliary fluids. It was found that stepping the mass flowrates induced instability of the solution on the scale of the global solver. This was overcome by modifying the time-step size based on the severity of the mass flow gradients. These steps occurred at different times of the simulation in order to see the effect of each. Table 5 is a summary of transient step inputs.

Table 5

Transient step inputs for Case 2

Condition	Auxiliary fluid		Primary fluid	
	T (°C)	Mass flow (kg/s)	*T* (°C)	Mass flow (kg/s)
Initial	150	1.5	5	2.58
Final	130	2	15	1.58
Occurring time (s)	10	15	0	5

From Fig. 13, it is evident that the results match very well. Stepping the mass flow has an immediate effect on the outlet temperatures of both fluids. This is due to the convection coefficients that are instantaneously stepped with the step in the incompressible fluid mass flowrate. Conversely, the temperature steps lag substantially as the fluid propagates from the inlet to the outlet in either the tubes or shell. The results agree very well with each other, especially the primary fluid's transient behavior. The auxiliary fluid resulted in a small offset near the final steady-state conditions which is a result of the inherent error.

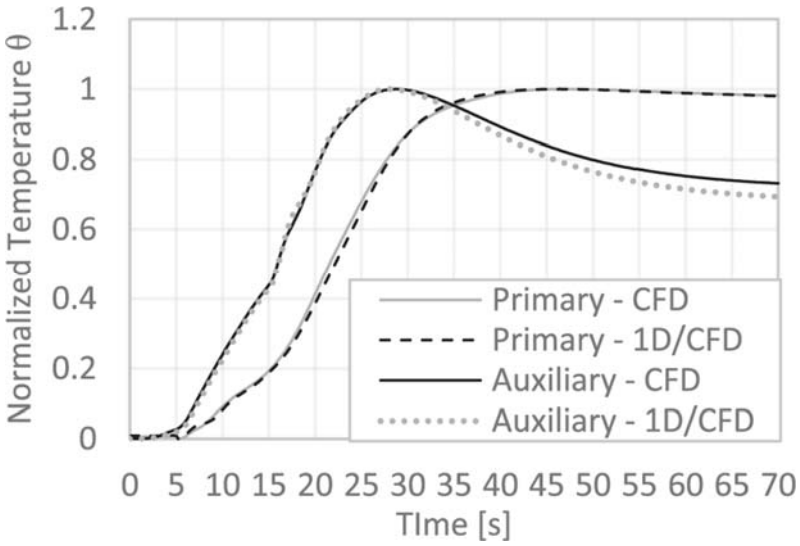

Fig. 13. Normalized transient results for multiple-step inputs

5 Conclusion

The development of the coupled 1D-CFD method was tested on a TEMA-FU-type STHX model and validated with a full CFD model. Results compared very well over a wide range of parameters, and the methodology is deemed effective for simplifying the analysis of flow-through tube bundles.

Acknowledgment

The authors gratefully acknowledge the support from the Eskom Power Plant Engineering Institute (EPPEI).

Nomenclature

d = inner diameter
f = Darcy friction factor
h = convection coefficient
n = exponent
r = radius
t = thickness
v = local velocity
D = shell diameter
I = turbulence intensity
L = length
K = pressure coefficient
Q = heat transfer rate
T = temperature
V = mean velocity
ξ = relaxation coefficient
ρ = density
τ_0 = local shear stress
Nu = Nusselt Number
Re = Reynolds Number
Pr = Prandtl Number

References

1) Hoseinzadeh, S., and Heyns, P. S., 2020, "Thermo-structural Fatigue and Lifetime Analysis of a Heat Exchanger as a Feedwater Heater in Power Plant," Eng. Fail. Anal., 113, p. 104548.
2) Liu, M. S., Dong, Q. W., Wang, D. B., and Ling, X., 1999, "Numerical Simulation of Thermal Stress in Tube-Sheet of Heat Transfer Equipment," Int. J. Press. Vessel. Pip., 76(10), pp. 671–675.
3) Li, H., Qian, C., and Yu, X., 2011, "Thermal Stress Analysis of a Tubesheet With a Welding Clad," Advanced Materials Research, 201–203, pp. 302–307.
4) Patil, R., and Anand, S., 2017, "Thermo-structural Fatigue Analysis of Shell and Tube Type Heat Exchanger," Int. J. Press. Vessel. Pip., 155, pp. 35–42.
5) Jiuyi, L., Caifu, Q., and Huifang, L., 2018, "Thermal Stress Analysis on the Thick Tubesheet With Square Layout of Tubes," Int. J. Interact. Des. Manuf., 12(1), pp. 243–251.
6) Mao, J., Tang, D., Bao, S., Luo, L., and Gao, Z., 2016, "High Temperature Strength and Multiaxial Fatigue Life Assessment of a Tubesheet Structure," Eng. Fail. Anal., 68, pp. 10–21.
7) Filimonov, S. A., Mikhienkova, E. I., Dekterev, A. A., and Boykov, D. V., 2017, "Hybrid Methods for Simulating Hydrodynamics and Heat Transfer in Multiscale (1D-3D) Models," J. Phys. Conf. Ser., 899(5), p. 052004.
8) Singh, S., and Abbassi, H., 2018, "1D/3D Transient HVAC Thermal Modeling of an Off-Highway Machinery Cabin Using CFD-ANN Hybrid Method," Appl. Therm. Eng., 135, pp. 406–417.
9) Zaversky, F., Sánchez, M., and Astrain, D., 2014, "Object-Oriented Modeling for the Transient Response Simulation of Multi-pass Shell-and-Tube Heat Exchangers as Applied in Active Indirect Thermal Energy Storage Systems for Concentrated Solar Power," Energy, 65, pp. 647–664.

10) Rousseau, P. G., and Gwebu, E. Z., 2018, “Modelling of a Superheater Heat Exchanger With Complex Flow Arrangement Including Flow and Temperature Maldistribution,” Heat Transf. Eng, 40(11), pp. 862–878.
11) Bonilla, J., de la Calle, A., Rodríguez-García, M. M., Roca, L., and Valenzuela, L., 2017, “Study on Shell-and-Tube Heat Exchanger Models With Different Degree of Complexity for Process Simulation and Control Design,” Appl. Therm. Eng., 124, pp. 1425–1440.
12) You, Y., Fan, A., Huang, S., and Liu, W., 2012, “Numerical Modeling and Experimental Validation of Heat Transfer and Flow Resistance on the Shell Side of a Shell-and-Tube Heat Exchanger With Flower Baffles,” Int. J. Heat Mass Transf., 55(25–26), pp. 7561–7569.
13) Ambekar, A. S., Sivakumar, R., Anantharaman, N., and Vivekenandan, M., 2016, “CFD Simulation Study of Shell and Tube Heat Exchangers With Different Baffle Segment Configurations,” Appl. Therm. Eng., 108, pp. 999–1007.
14) Kim, J., Sibilli, T., Ha, M. Y., Kim, K., and Yoon, S. Y., 2019, “Compound Porous Media Model for Simulation of Flat Top U-Tube Compact Heat Exchanger,” Int. J. Heat Mass Transf., 138, pp. 1029–1041.
15) Kruger, J., and Du Toit, C., 2006, “The Simulation of a Thermal-Fluid System Using an Integrated Systems CFD Approach,” Fifth International Conference on CFD in the Process Industries CSIRO, Melbourne, Australia, pp. 1–7.
16) Koekemoer, O., Du Toit, C., and Kruger, J., 2018, Investigation Into the Coupled 1D and 3D Numerical Modeling of an Air-Cooled Heat Exchanger Configuration OC Koekemoer, North-West University, Potchefstroom Campus, South Africa.
17) Flownex, S. E., 2015, “Flownex Theory Manual.”
18) Ansys, 2019, Ansys Fluent Theory Guide.
19) Verstraete, T., and Van den Braembussche, R. A., 2009, “A Novel Method for the Computation of Conjugate Heat Transfer With Coupled Solvers,” International Symposium on Heat Transfer in Gas Turbine Systems, Antalya.
20) Roache, P. J., 1998, Verification and Validation in Computational Science and Engineering, Hermosa Publishers, Albuquerque, NM.